

Comparative performance of ^{18}F -FDG PET/MRI and ^{18}F -FDG PET/CT regarding detection and characterization of pulmonary lesions in 121 oncologic patients

Lino M Sawicki^{1,2}, Johannes Grueneisen², Christian Buchbender¹, Benedikt M Schaarschmidt¹, Benedikt Gomez³, Verena Ruhlmann³, Axel Wetter², Lale Umutlu², Gerald Antoch¹, Philipp Heusch¹

¹University Dusseldorf, Medical Faculty, Department of Diagnostic and Interventional Radiology, D-40225 Dusseldorf, Germany

²University Duisburg-Essen, Medical Faculty, Department of Diagnostic and Interventional Radiology and Neuroradiology, Essen, Germany

³University Duisburg-Essen, Medical Faculty, Department of Nuclear Medicine, D-45147 Essen, Germany

Corresponding author:

Lino Sawicki

University Dusseldorf, Medical Faculty, Department of Diagnostic and Interventional Radiology

D-40225 Dusseldorf, Germany

Tel: +49 (0) 211 - 811 77 54

Telefax: +49 (0) 211 - 8 11 61 45

E-mail: linomorris.sawicki@med.uni-duesseldorf.de

First author:

Lino Sawicki

MD, resident

University Dusseldorf, Medical Faculty, Department of Diagnostic and Interventional
Radiology

Moorenstrasse 5

D-40225 Dusseldorf, Germany

Tel: +49 (0) 211 - 811 77 54

Telefax: +49 (0) 211 - 8 11 61 45

E-mail: linomorris.sawicki@med.uni-duesseldorf.de

Word count: 4985

No financial support was provided for this work.

Nothing to disclose.

No conflicts of interest.

Running title: PET/MRI vs. PET/CT in lung lesions

ABSTRACT

To compare ^{18}F -fluorodesoxyglucose positron emission tomography/magnetic resonance imaging (^{18}F -FDG PET/MRI) using a contrast-enhanced T1-weighted (T1w) fat-suppressed (fs) volume-interpolated breath-hold examination (VIBE) sequence with ^{18}F -FDG PET/computed tomography (^{18}F -FDG PET/CT) regarding detection and characterization of lung lesions in oncologic patients.

Methods: 121 oncologic patients underwent PET/MRI following PET/CT in a single-injection protocol (260 ± 58 MBq ^{18}F -FDG). Lung lesion detection rates of T1w fs VIBE, PET from ^{18}F -FDG PET/CT, and PET from ^{18}F -FDG PET/MRI were computed in relation to the CT component of PET/CT. Wilcoxon tests assessed differences in lesion contrast (four-point scale) and lesion size between morphologic datasets as well as in image quality (four-point scale), mean and maximum standard uptake values (SUV_{mean}, SUV_{max}), and dignity ratings (benign/malignant) between ^{18}F -FDG PET/MRI and ^{18}F -FDG PET/CT. Correlations were calculated using Pearson's coefficients (r) for SUV and size and Spearman's rank coefficient (ρ) for lesion contrast.

Results: Detection rates of T1w fs VIBE, PET from ^{18}F -FDG PET/CT and PET from ^{18}F -FDG PET/MRI regarding 241 lung lesions were 66.8%, 42.7%, and 42.3%, respectively. There was a strong correlation in size ($r=0.98$) and SUVs ($r=0.91$) and a moderate correlation concerning lesion contrast ($\rho=0.48$). Image quality of ^{18}F -FDG PET/MRI was inferior to ^{18}F -FDG PET/CT ($p<0.001$). Corresponding lung lesions were measured smaller on T1w fs VIBE than on CT ($p<0.001$). SUV_{max} and SUV_{mean} from ^{18}F -FDG PET/MRI were significantly higher than from ^{18}F -FDG PET/CT ($p<0.001$ each). There was no significant difference in lesion contrast ($p=0.11$) or dignity ratings ($p=0.076$).

Conclusion: Performance of ^{18}F -FDG PET/MRI regarding detection and characterization of lung lesions ≥ 10 mm is comparable to ^{18}F -FDG PET/CT. Lesion size, SUV and dignity ratings correlate strongly. However, the overall detection rate of ^{18}F -FDG PET/MRI remains inferior to ^{18}F -FDG PET/CT due to the limited detectability of lesions < 10 mm on T1w fs VIBE. Thus, thoracic staging with ^{18}F -FDG PET/MRI bears a risk of missing small lung metastases.

Key words: lung, lesion, MRI, PET/MRI, PET/CT

INTRODUCTION

Pulmonary lesion detection and assessment of dignity play a key role in cancer staging as the presence of lung metastases influences therapy regimens and patient survival (1-3). Computed tomography (CT) has been regarded as the reference standard for lung lesion detection offering high spatial resolution of the pulmonary tissue (4,5). However, since morphologic CT-based criteria have a relatively low specificity in lung lesion dignity there has been a need for a more robust diagnostic standard. Over the last decade ¹⁸F-fluorodesoxyglucose positron emission tomography/CT (¹⁸F-FDG PET/CT) has proven successful not only in pulmonary lesion detection but also in the discrimination of benign and malignant findings taking advantage of the accurate anatomic information from CT and functional characteristics from PET in a one-stop shop examination (6-8). Yet, a major drawback of ¹⁸F-FDG PET/CT involves the low sensitivity of the PET component in pulmonary lesions < 10 mm owing to motion artifacts and partial volume effects as well as its limited spatial resolution (9). Magnetic resonance imaging (MRI) has only played a minor role in radiologic assessment of the lung, mainly due to methodological and physical shortcomings, such as low proton density in aerated lungs, fast decay of signal, and motion artifacts caused by breathing and cardiac pulsation. Comparing different MRI sequences, T1-weighted (T1w) 3 dimensional (3D) gradient echo (GRE) sequences, such as T1w volume-interpolated breath-hold examination (VIBE), demonstrate the highest sensitivity and are thus recommended for MR-based identification of pulmonary lesions (3-5). Nevertheless, several studies indicated that lesion detection in MRI remains inferior to CT (4,10,11). Recently introduced, fully integrated whole-body PET/MRI combines simultaneously acquired metabolic PET information with high soft-tissue contrast images and functional information obtained by MRI to allow for an improved assessment of tumor burden in cancer patients (12-14). Bearing in

mind the challenges of MRI in pulmonary imaging, the increasing utilization of whole-body PET/MRI has sparked renewed interest in its performance in lung lesion depiction. Herein, not only the comparison of morphologic imaging datasets (MRI vs. CT) but also the performance of PET from ^{18}F -FDG PET/MRI vs. PET from ^{18}F -FDG PET/CT is of great interest considering the differences in PET acquisition and attenuation correction techniques. Existing evidence in this field is based on a study by Rauscher et al. and another study by Chandarana et al. of which the former comprised 40 patients, the latter 32 patients (15,16).

Thus, the purpose of our study was to compare ^{18}F -FDG PET/MRI using T1w VIBE as the morphologic dataset with ^{18}F -FDG PET/CT regarding lung lesion detection and characterization in a larger cohort of oncologic patients.

MATERIALS AND METHODS

Patients and inclusion criteria

All patients with proven or suspected malignancies (TABLE 1) who underwent ^{18}F -FDG PET/MRI including a contrast-enhanced T1w fat-suppressed (fs) VIBE sequence of the thorax following a clinically scheduled ^{18}F -FDG PET/CT for staging purposes on the same day were included in this study. Accordingly, a total of 121 subjects (mean age: 57.1 ± 13.9 years; 71 female, 50 male) between May 2012 and December 2014 were eligible for retrospective analysis. This study has been approved by the local ethics committee and all subjects signed an informed consent form.

PET/CT Imaging

Whole-body ^{18}F -FDG PET/CT was performed on a Biograph mCT or Biograph Duo scanner (Siemens Healthcare GmbH, Erlangen, Germany) 61 ± 10.3 minutes after

intravenous injection of a mean activity of 260 ± 58 MBq ^{18}F -FDG, depending on patients' body weight. Blood glucose levels were verified to be below 150 mg/dl at injection time. Patients were examined in full-dose ($n = 67$) and low-dose ($n = 54$) technique. In full-dose scans an iodinated contrast medium was administered (Imeron 300, Bracco Imaging Deutschland GmbH, Konstanz, Germany) and an additionally acquired dedicated low-dose lung scan applying a sharp b 70 or b 90 kernel in deep inspiration was performed. All CT images were displayed using a transverse lung window setting with a slice thickness of 2 mm. Manufacturer-supplied dose reduction software CareKV and CareDose 4D was available for both full-dose and low-dose ^{18}F -FDG PET/CT scans (presets: 120 kV; 210 mAs and 120 kV; 40 mAs, respectively). PET-acquisition time using static frames varied from 2 – 3.5 minutes per bed position with an average of seven bed positions necessary to cover the body volume. Iterative reconstruction (three iterations, 21 subsets) and a Gaussian filter of 4 mm were applied. In general, PET images were reconstructed with a slice thickness of 3 mm. The portal venous phase of full-dose CT scans and low-dose CT data in low-dose scans were used for attenuation correction of the PET images.

PET/MR Imaging

Whole-body ^{18}F -FDG PET/MRI using flex coils was performed on a 3 Tesla Biograph mMR scanner (Siemens Healthcare GmbH, Erlangen, Germany). Following ^{18}F -FDG-PET/CT with the shortest possible delay ^{18}F -FDG PET/MRI scans began 113.9 ± 28.5 minutes after radiotracer injection. First, a coronal 3D-Dixon-VIBE sequence (repetition time (TR) 3.6 ms, echo time 1 (TE1) 1.23 ms, TE2 2.46 ms, slice thickness 3.12 mm, FOV 500 x 328 mm, matrix size 192 x 121, voxel size: 4.1 x 2.6 x 3.1 mm) was acquired to generate an attenuation map for MR-based attenuation correction. Then, dedicated MRI protocols were

performed in each patient depending on clinical implications. A transverse T1w fs VIBE sequence (TR 4.08 ms, TE 1.51 ms, slice thickness 3.5 mm, FOV 400 x 300 mm, matrix size 512 x 307.2, voxel size: 1.3 x 0.8 x 3.5 mm) after administration of a gadolinium-based contrast medium (Dotarem, Guerbet GmbH, Sulzbach, Germany) served as the only morphological dataset for lung assessment in this study and was used for PET/MR image fusion. For imaging of the thorax the contrast-enhanced T1w fs VIBE sequence was acquired during breath-hold in deep inspiration. Generalized autocalibrating partially parallel acquisitions with an acceleration factor of two were applied to increase acquisition speed. In general, PET acquisition time was 3 minutes per bed position (two bed positions for the whole thorax) starting simultaneously with 3D-Dixon-VIBE sequence acquisition. PET images were acquired in list mode and reconstructed in the same way as in ^{18}F -FDG PET/CT using iterative algorithm ordered-subsets expectation maximization with three iterations and 21 subsets, a Gaussian filter of 4 mm and a slice thickness of 3 mm.

Image analysis

All imaging datasets were evaluated on an OsiriX Workstation (Pixmeo SARL, Bernex, Switzerland) and independently analyzed by two radiologists with three and four years of experience in PET/CT and PET/MRI interpretation. Any discrepancies between the two readers were resolved in a subsequent consensus reading. Readers were blinded to the patients' history. ^{18}F -FDG PET/CT and ^{18}F -FDG PET/MRI were assessed in separate sessions and in random order with a minimum of four weeks apart to avoid recognition bias. Morphologic chest images (T1w fs VIBE and CT) as well as PET from ^{18}F -FDG PET/CT and PET from ^{18}F -FDG PET/MRI were analyzed separately and as fused ^{18}F -FDG PET/CT and ^{18}F -FDG PET/MRI datasets. PET images were reviewed with and without attenuation

correction to prevent false-positive findings caused by attenuation-correction artifacts. Readers evaluated the image quality of each fused ^{18}F -FDG PET/CT and ^{18}F -FDG PET/MRI using a four-point scale (1 = very poor image quality: major artifacts, no diagnostic value; 2 = poor image quality: distinct artifacts, considerably limited diagnostic use; 3 = good image quality: minor artifacts, marginally limited diagnostic use; 4 = excellent image quality: no artifacts, unconditional diagnostic use). As previously described by Rauscher et al. (16), CT and PET from ^{18}F -FDG PET/CT as well as contrast-enhanced T1w fs VIBE and PET from ^{18}F -FDG PET/MRI were assessed separately with regard to the presence and the number of lung lesions, where the CT component of ^{18}F -FDG PET/CT served as the standard of reference. A maximum of ten lung lesions was identified for each patient, starting from the right upper lobe proceeding to the left lower lobe. Lesion size (longitudinal axis diameter) in mm was measured on T1w fs VIBE and CT. Qualitative assessment of lesion contrast on T1w fs VIBE and CT was performed using a four-point scale (1 = very low contrast; 2 = low contrast; 3 = moderate contrast; 4 = high contrast). Presence of focal tracer uptake above the surrounding background (morphologically unaltered lung tissue) was noted for each lung lesion. For quantitative assessment and comparison of tracer uptake, mean and maximum standard uptake values (SUVmean, SUVmax) were evaluated by placing a freehand polygonal volume of interest (VOI) over each lung lesion on corresponding attenuation-corrected PET from ^{18}F -FDG PET/CT and ^{18}F -FDG PET/MRI. Osirix Software automatically calculated SUVmean and SUVmax from VOIs on PET images. Each lung lesion was rated regarding its presumed dignity (1 = most likely benign; 2 = indeterminate; 3 = suspicious for malignancy). Determination of dignity was based on the presence of a focal FDG uptake and typical morphological criteria in benign and malignant pulmonary nodules as established by Seemann et al. (17,18).

Statistics

IBM SPSS Statistics 22 (IBM, Armonk, NY, USA) was used for statistical analysis. All data are given as mean \pm standard deviation. A p-value (p) of < 0.05 was considered to be statistically significant. Data were tested for normal distribution using a Kolmogorov-Smirnov test. Descriptive analysis was performed. Wilcoxon tests were used to evaluate differences in SUVmean, SUVmax, size, image quality, lesion contrast, and dignity ratings. Correlation between ^{18}F -FDG PET/MRI and ^{18}F -FDG PET/CT was assessed using Pearson's correlation coefficients (r) for SUVmean, SUVmax and size and Spearman's rank correlation coefficient (ρ) for lesion contrast and dignity ratings, respectively. Detection rates were calculated by dividing the respective total of lung lesions detected on T1w fs VIBE, PET from ^{18}F -FDG PET/CT, and PET from ^{18}F -FDG PET/MRI by the total of lung lesions found on the CT component of PET/CT as the reference standard.

RESULTS

Lesion detection

According to the standard of reference a total of 241 lung lesions measuring 13.1 ± 15.2 mm (range: 1 - 98 mm) were found in 84 out of 121 patients. Contrast-enhanced T1w fs VIBE showed an overall detection rate of 66.8 %. The detection rates of contrast-enhanced T1w fs VIBE for lung lesions < 10 mm, < 5 mm, and ≥ 10 mm were 45.9 %, 43.1 %, and 94.9 %, respectively. A separate evaluation of T1w fs VIBE detection rates with respect to either low-dose lung scans performed in deep inspiration as part of the full-dose PET/CT protocol or low-dose lung scans performed in shallow breathing from low-dose PET/CT yielded detection rates of 62.1 % and 72.5 %, respectively, suggesting that more lung lesions were missed on

T1w fs VIBE when compared to CT in deep inspiration. However, a MWU test showed that the average number of missed lesions on T1w fs VIBE vs. CT in deep inspiration (0.75 ± 1.11) and CT in shallow breathing (0.56 ± 1.25) did not differ significantly ($p = 0.146$). Resolution limits for lung lesions were 1 mm on CT and 3 mm on contrast-enhanced T1w fs VIBE. The PET components of ^{18}F -FDG PET/CT and of ^{18}F -FDG PET/MRI demonstrated focal tracer uptake in 42.7 % and 42.3 % of all lung lesions, respectively. There was no focal ^{18}F -FDG uptake on PET images from PET/MRI or PET/CT that did not correspond to a visual morphologic correlate on contrast-enhanced T1w fs VIBE or CT, respectively. Hence, the detection rate of fused ^{18}F -FDG PET/MRI and ^{18}F -FDG PET/CT was identical to that of its respective morphologic imaging component. FIGURES 1 and 2 show different examples of lung lesions on ^{18}F -FDG PET/CT and ^{18}F -FDG PET/MRI.

Comparison of lesion size and lesion contrast

Analysis of lesion size revealed that corresponding lung lesions detected on both contrast-enhanced T1w fs VIBE and CT ($n = 161$) were measured significantly smaller ($p < 0.001$) on contrast-enhanced T1w fs VIBE (average size: 17.1 ± 16.8 mm) than on CT (17.7 ± 16.9 mm). The smaller size of corresponding lung lesions on contrast-enhanced T1w fs VIBE was a constant phenomenon, thus, there was a strong correlation in lesion size between both modalities ($r = 0.98$; $p < 0.001$). For a linear regression analysis and a Bland–Altman plot, see FIGURE 3. A high average lesion contrast of corresponding lung lesions was found on CT (3.65 ± 0.6) and contrast-enhanced T1w fs VIBE images (3.61 ± 0.7). There was no significant difference ($p = 0.11$) and a moderate positive correlation regarding corresponding lung lesion contrast between CT and contrast-enhanced T1w fs VIBE ($p = 0.48$; $p < 0.001$).

Quantitative assessment of SUV

The average SUVmax and SUVmean from ^{18}F -FDG PET/MRI was significantly higher than the respective average SUVs from ^{18}F -FDG PET/CT in 96 corresponding PET-positive lung lesions detected on both modalities (average SUVmax from ^{18}F -FDG PET/MRI = 7.39 ± 6.7 , average SUVmax from ^{18}F -FDG PET/CT = 6.09 ± 6.5 ; average SUVmean from ^{18}F -FDG PET/MRI 3.73 ± 2.9 , average SUVmean from ^{18}F -FDG PET/CT 3.3 ± 2.9 ; $p < 0.001$ each). A strong positive correlation was found for SUVmax ($r = 0.91$; $p < 0.001$) and SUVmean ($r = 0.91$; $p < 0.001$) from both hybrid imaging modalities. A Bland–Altman plot illustrating differences in SUV measurements from ^{18}F -FDG PET/CT and ^{18}F -FDG PET/MRI can be found in FIGURE 4.

Dignity rating

On both modalities the majority of lung lesions was rated as either most likely benign or suspicious for malignancy, while only a small proportion was rated indeterminate. Since the number of lung lesions detected with ^{18}F -FDG PET/MRI was smaller than the number of lesions detected with ^{18}F -FDG PET/CT and contrast-enhanced T1w fs VIBE mainly detected larger lesions, a greater proportion of lung lesions was classified as suspicious of malignancy with ^{18}F -FDG PET/MRI than with ^{18}F -FDG PET/CT (66 % vs. 41 %). Ratings of the 161 corresponding lung lesions that were found both on ^{18}F -FDG PET/CT and ^{18}F -FDG PET/MRI did not differ significantly from each other ($p = 0.076$) and showed a significantly strong correlation ($\rho = 0.87$; $p < 0.001$). Dignity ratings of all pulmonary lesions are shown in TABLE 2.

Image quality

The mean image quality of both fused ^{18}F -FDG PET/MRI and ^{18}F -FDG PET/CT was rated as “good” to “excellent”. However, a Wilcoxon test yielded a significantly lower mean image quality of ^{18}F -FDG PET/MRI compared with ^{18}F -FDG PET/CT (3.5 ± 0.5 vs. 3.7 ± 0.5 ; $p < 0.001$).

DISCUSSION

The results of our study indicate that detection rates of ^{18}F -FDG PET/MRI and ^{18}F -FDG PET/CT are nearly equivalent in pulmonary lesions ≥ 10 mm. However, detectability of lung lesions < 10 mm on ^{18}F -FDG PET/MRI remains inferior even when applying currently recommended T1w 3D volume-interpolated GRE sequences such as contrast-enhanced T1w fs VIBE as the morphologic dataset. PET datasets of ^{18}F -FDG PET/MRI and ^{18}F -FDG PET/CT delivered comparable results.

Considering the nearly equivalent performance of both hybrid imaging modalities in lung lesions ≥ 10 mm and that dignity ratings did not vary significantly, our study seems to support the general applicability of ^{18}F -FDG PET/MRI as an alternative to ^{18}F -FDG PET/CT in the staging tumors metastasizing to the lung. The applicability of ^{18}F -FDG PET/MRI is substantiated by the fact that both hybrid imaging modalities showed “good” to “excellent” image quality and corresponding lung lesion contrast was similar. However, as T1w fs VIBE missed more than half of pulmonary lesions $< 10\text{mm}$, the overall diagnostic performance of T1w fs VIBE of ^{18}F -FDG PET/MRI was still outmatched by the CT component of ^{18}F -FDG PET/CT. Because only one third of the lung consists of tissue and two thirds of air, proton density is substantially lower in the lung than in any other human organ. Rapid signal loss and motion artifacts from cardiac or aortic pulsation as well as from breathing are additional factors impairing the signal-to-noise ratio in MRI. By effectively exploiting the signal from

available protons, T1w GRE sequences (e. g. VIBE) with short TE (< 7 ms) have proven superior in lung lesion depiction compared to longer TE, spin echo or pulse sequences and are thus recommended for MR-based lesion detection (19). Reasons for ¹⁸F-FDG PET/MRI's inferiority are found in methodological shortcomings of MRI in depicting small lung nodules, which accounted for the majority of lesions in our study. Former studies by Sommer et al., Biederer et al., and Muller et al. evaluating CT and MRI corroborate these findings (4,10,11). Moreover, two recently published studies by Rauscher et al. and Chandarana et al. comparing ¹⁸F-FDG PET/MRI and ¹⁸F-FDG PET/CT yielded similar detection rates of T1w VIBE images of 68 % and 70 % compared to diagnostic CT (15,16). The clinical impact of this finding, however, remains controversial as the majority of small pulmonary nodules are known to be non-cancerous even in patients with a proven malignancy (20). Nevertheless, the presence of early-stage lung metastases cannot be excluded and the risk of a missed metastatic spread has to be considered performing ¹⁸F-FDG PET/MRI solely. Thus, further development towards more sensitive MR sequences seems required for PET/MRI to be accepted as an independent staging modality. In patients with proven or suspected malignancy FDG-avid lung lesions are generally considered as suspicious of malignancy. As a result of the nearly equivalent performance of both PET components and the lower number of small lung lesions identified on T1w fs VIBE, a greater proportion of lung lesions rated as malignant would be expected using ¹⁸F-FDG PET/MRI compared with ¹⁸F-FDG PET/CT. This was substantiated by our study showing 25 % more lesions suspicious of malignancy on ¹⁸F-FDG PET/MRI than on ¹⁸F-FDG PET/CT.

In concordance with prior studies we observed a strong positive correlation between SUV measurements (15,16,21). Additionally, we could confirm the propensity for slightly higher SUVs measured on ¹⁸F-FDG PET/MRI compared to ¹⁸F-FDG PET/CT (15,16,22,23).

Underlying reasons are not yet completely understood but it is assumed that besides differences in scanner technology, biologic factors might play a role. Since patients first underwent ^{18}F -FDG PET/CT there was a longer interval between ^{18}F -FDG PET/MRI and radiotracer injection (114 minutes vs. 61 minutes). Tissues with a high glucose turnover such as lung metastases are hypothesized to have an increased intracellular tracer trapping on delayed time-point images (24,25).

Although we found a strong positive correlation regarding size measurements, there was a significant tendency of corresponding pulmonary lesions to be measured smaller on ^{18}F -FDG PET/MRI than on ^{18}F -FDG PET/CT. This, again, is probably due to technical differences between both morphological datasets. While the higher spatial resolution of CT allows for a precise lesion depiction, at the same time, the fast decay of MR signal at air-tissue interfaces may compromise detailed imaging at the periphery of a lesion (19).

Our study has some limitations. First, we did not evaluate other MR sequences such as T2w single-shot turbo spin echo or radial blade sequences. While the assessment of a multi-sequence MR protocol might arguably increase the detection rate of ^{18}F -FDG PET/MRI, the potential improvement would probably be marginal as T1w 3D volume-interpolated GRE sequences offer the highest sensitivity especially in small pulmonary lesions, whereas T2w pulmonary imaging is more adequate for the visualization of infiltrates or adjacent structures like the mediastinum (26). A second limitation was the use of two different ^{18}F -FDG PET/CT protocols (one with additional low-dose CT of the chest in deep inspiration, the other one without) that may have led to an underestimation of the total number of lung nodules on the reference standard. However, our data suggest that ^{18}F -FDG PET/CT with a lung scan in deep inspiration does not identify significantly more missed lung lesions than one performed in shallow breathing.

CONCLUSION

Our study has shown that ^{18}F -FDG PET/MRI of the thorax has high image quality with similar detection rates compared to ^{18}F -FDG PET/CT in pulmonary lesions ≥ 10 mm, thus supporting the general applicability of ^{18}F -FDG PET/MRI as an alternative to ^{18}F -FDG PET/CT in the staging of oncologic patients. Notwithstanding technical differences, detection rates of the PET datasets from both hybrid imaging modalities are comparable. Furthermore, there is a strong positive correlation regarding lesion size, SUVmax, and SUVmean as well as dignity ratings between ^{18}F -FDG PET/MRI and ^{18}F -FDG PET/CT. However, the overall detection rate of ^{18}F -FDG PET/MRI remains inferior to that of ^{18}F -FDG PET/CT owing to the lower detectability of pulmonary lesions < 10 mm on T1w 3D volume-interpolated GRE sequences. Hence, tumor staging with ^{18}F -FDG PET/MRI bears a risk of missing small lung metastases. Thus, further research on more sensitive MR sequences seems required.

DISCLOSURE

No financial support was provided for this work. There were no conflicts of interest.

ACKNOWLEDGEMENTS

None.

REFERENCES

1. Edge SB, Byrd DR, Compton CC, Fritz AG, Greene FL, Trotti A. *AJCC cancer staging manual*. 7th ed. New York, NY: Springer; 2010.
2. Barth A, Wanek LA, Morton DL. Prognostic factors in 1,521 melanoma patients with distant metastases. *J Am Coll Surg*. 1995;181:193-201.
3. Biederer J, Beer M, Hirsch W, et al. MRI of the lung (2/3). Why ... when ... how? *Insights Imaging*. 2012;3:355-371.
4. Sommer G, Koenigkam-Santos M, Biederer J, Puderbach M. Role of MRI for detection and characterization of pulmonary nodules. *Radiologe*. 2014;54:470-477.
5. Biederer J, Hintze C, Fabel M. MRI of pulmonary nodules: technique and diagnostic value. *Cancer Imaging*. 2008;8:125-130.
6. Cistaro A, Lopci E, Gastaldo L, Fania P, Brach Del Prever A, Fagioli F. The role of 18F-FDG PET/CT in the metabolic characterization of lung nodules in pediatric patients with bone sarcoma. *Pediatr Blood Cancer*. 2012;59:1206-1210.
7. Dabrowska M, Krenke R, Korczynski P, et al. Diagnostic accuracy of contrast-enhanced computed tomography and positron emission tomography with 18-FDG in identifying malignant solitary pulmonary nodules. *Medicine (Baltimore)*. 2015;94:e666.
8. Opoka L, Kunikowska J, Podgajny Z, et al. Accuracy of FDG PET/CT in the evaluation of solitary pulmonary lesions - own experience. *Pneumonol Alergol Pol*. 2014;82:198-205.
9. Tan BB, Flaherty KR, Kazerooni EA, Iannettoni MD. The solitary pulmonary nodule. *Chest*. 2003;123:89-96.
10. Biederer J, Schoene A, Freitag S, Reuter M, Heller M. Simulated pulmonary nodules implanted in a dedicated porcine chest phantom: sensitivity of MR imaging for detection. *Radiology*. 2003;227:475-483.
11. Muller NL, Gamsu G, Webb WR. Pulmonary nodules: detection using magnetic resonance and computed tomography. *Radiology*. 1985;155:687-690.
12. Drzezga A, Souvatzoglou M, Eiber M, et al. First clinical experience with integrated whole-body PET/MR: comparison to PET/CT in patients with oncologic diagnoses. *J Nucl Med*. 2012;53:845-855.
13. Buchbender C, Heusner TA, Lauenstein TC, Bockisch A, Antoch G. Oncologic PET/MRI, part 1: tumors of the brain, head and neck, chest, abdomen, and pelvis. *J Nucl Med*. 2012;53:928-938.

14. Buchbender C, Heusner TA, Lauenstein TC, Bockisch A, Antoch G. Oncologic PET/MRI, part 2: bone tumors, soft-tissue tumors, melanoma, and lymphoma. *J Nucl Med.* 2012;53:1244-1252.
15. Chandarana H, Heacock L, Rakheja R, et al. Pulmonary nodules in patients with primary malignancy: comparison of hybrid PET/MR and PET/CT imaging. *Radiology.* 2013;268:874-881.
16. Rauscher I, Eiber M, Furst S, et al. PET/MR imaging in the detection and characterization of pulmonary lesions: technical and diagnostic evaluation in comparison to PET/CT. *J Nucl Med.* 2014;55:724-729.
17. Seemann MD, Seemann O, Luboldt W, et al. Differentiation of malignant from benign solitary pulmonary lesions using chest radiography, spiral CT and HRCT. *Lung Cancer.* 2000;29:105-124.
18. Seemann MD, Staebler A, Beinert T, et al. Usefulness of morphological characteristics for the differentiation of benign from malignant solitary pulmonary lesions using HRCT. *Eur Radiol.* 1999;9:409-417.
19. Kauczor HU, Kreitner KF. Contrast-enhanced MRI of the lung. *Eur J Radiol.* 2000;34:196-207.
20. Benjamin MS, Drucker EA, McLoud TC, Shepard JA. Small pulmonary nodules: detection at chest CT and outcome. *Radiology.* 2003;226:489-493.
21. Heusch P, Buchbender C, Kohler J, et al. Thoracic staging in lung cancer: prospective comparison of 18F-FDG PET/MR imaging and 18F-FDG PET/CT. *J Nucl Med.* 2014;55:373-378.
22. Pace L, Nicolai E, Luongo A, et al. Comparison of whole-body PET/CT and PET/MRI in breast cancer patients: lesion detection and quantitation of 18F-deoxyglucose uptake in lesions and in normal organ tissues. *Eur J Radiol.* 2014;83:289-296.
23. Paspulati RM, Partovi S, Herrmann KA, Krishnamurthi S, Delaney CP, Nguyen NC. Comparison of hybrid FDG PET/MRI compared with PET/CT in colorectal cancer staging and restaging: a pilot study. *Abdom Imaging.* 2015;40:1415-1425.
24. Cheng G, Torigian DA, Zhuang H, Alavi A. When should we recommend use of dual time-point and delayed time-point imaging techniques in FDG PET? *Eur J Nucl Med Mol Imaging.* 2013;40:779-787.
25. Costantini DL, Vali R, Chan J, McQuattie S, Charron M. Dual-time-point FDG PET/CT for the evaluation of pediatric tumors. *AJR Am J Roentgenol.* 2013;200:408-413.
26. Fink C, Puderbach M, Biederer J, et al. Lung MRI at 1.5 and 3 Tesla: observer preference study and lesion contrast using five different pulse sequences. *Invest Radiol.* 2007;42:377-383.

FIGURE LEGENDS

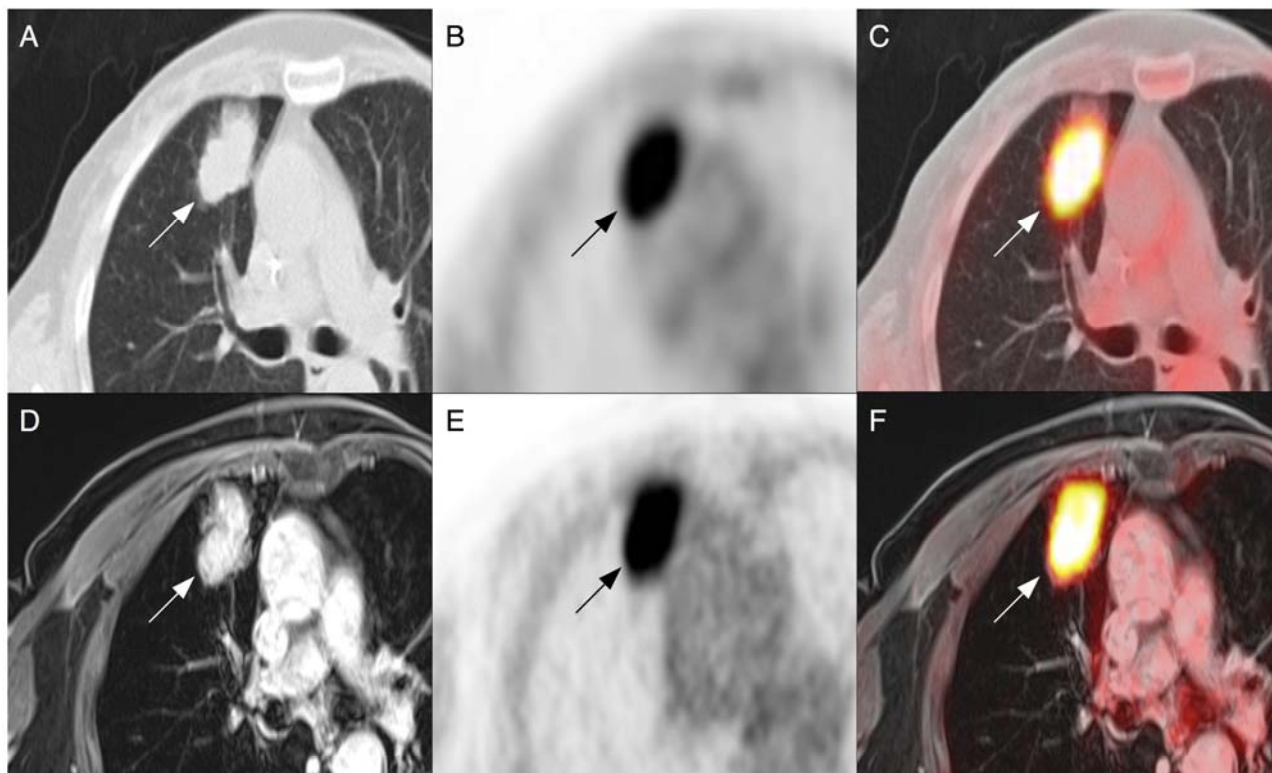


FIGURE 1. Images of a 65-year-old female patient with lung cancer. The tumor is identified as a 38 mm pulmonary mass (arrows in A – F) in the right upper lobe on the CT images (A) of ^{18}F -FDG PET/CT (C) and on the contrast-enhanced T1w fs VIBE images (D) of ^{18}F -FDG PET/MRI (F). Strong tracer uptake is attributable to the mass on PET from ^{18}F -FDG PET/CT (SUVmax 17.3) (B) and PET from ^{18}F -FDG PET/MRI (SUVmax 19.4) (E) as well as on fused images (C, F).

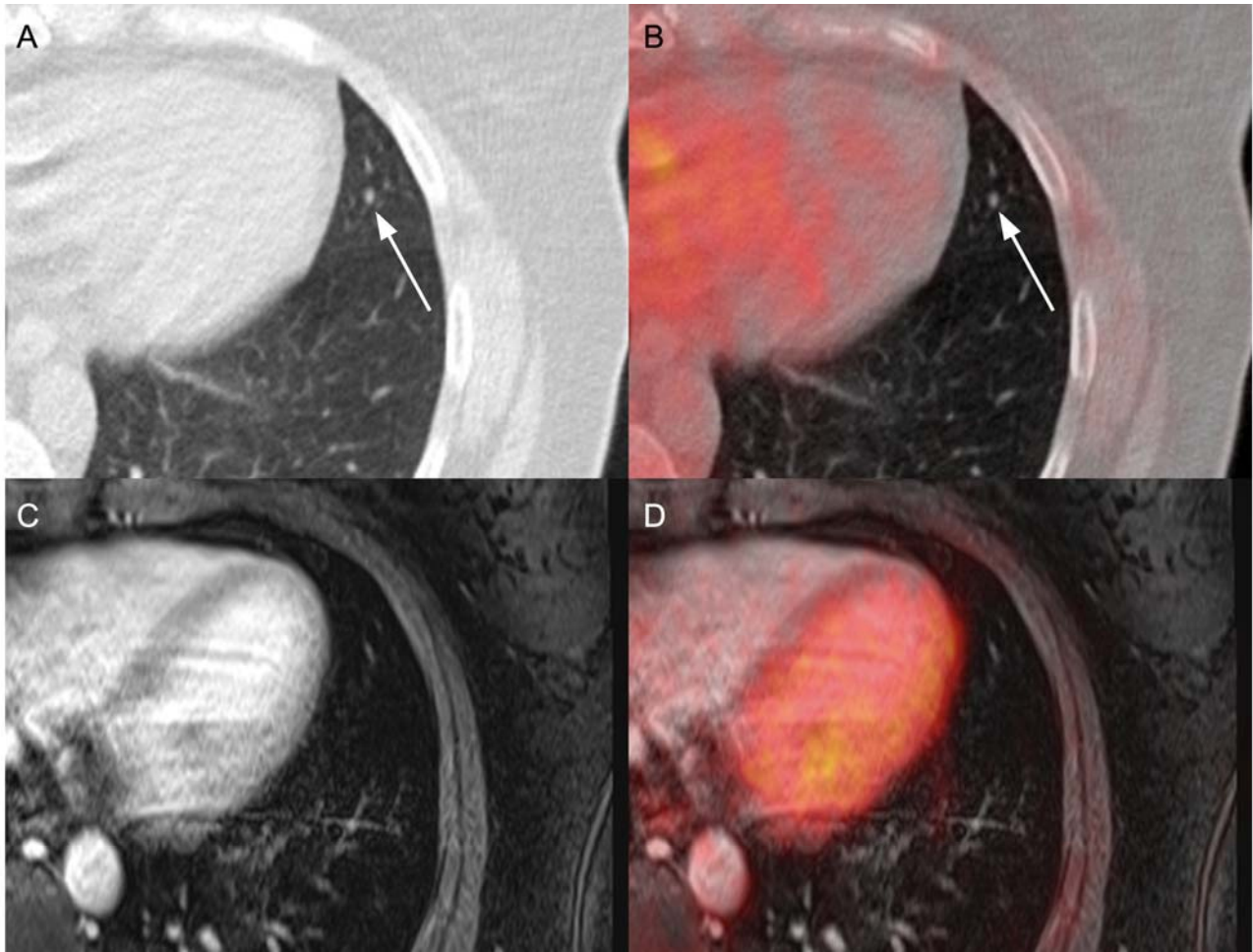


FIGURE 2. Images of a 46-year-old female patient with breast cancer. Four mm lung nodule in the lingula segment of the left upper lobe (arrows in A and B) detected on the CT component (A) of ^{18}F -FDG PET/CT (B) but not identifiable on contrast-enhanced T1w fs VIBE images (C) of ^{18}F -FDG PET/MRI (D). Corresponding PET from ^{18}F -FDG PET/CT (C) and PET from ^{18}F -FDG PET/MR (D) demonstrated no focal tracer uptake of the pulmonary nodule.

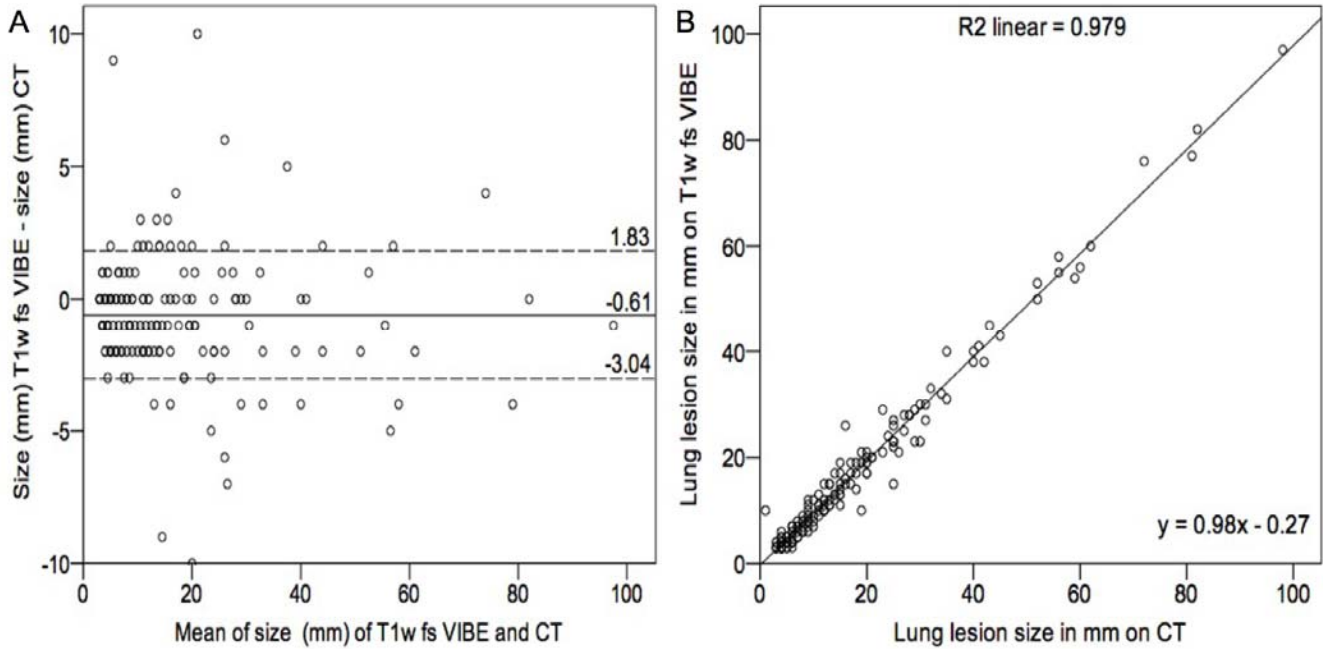


FIGURE 3. A) Difference in size of 161 corresponding lung lesions detected on T1w fs VIBE from ^{18}F -FDG PET/MRI and CT from ^{18}F -FDG PET/CT illustrated by a Bland-Altman plot. The difference between the two size measurements was plotted against their mean. The mean difference was -0.61 mm; 95 % confidence interval: 1.83 mm and -3.04 mm. B) Linear regression plot demonstrating the correlation of corresponding lung lesion size on T1w fs VIBE and CT. In conformity with the linear regression plot, a Pearson’s correlation analysis revealed that lung lesion size was strongly correlated between both modalities ($r = 0.98$; $p < 0.001$).

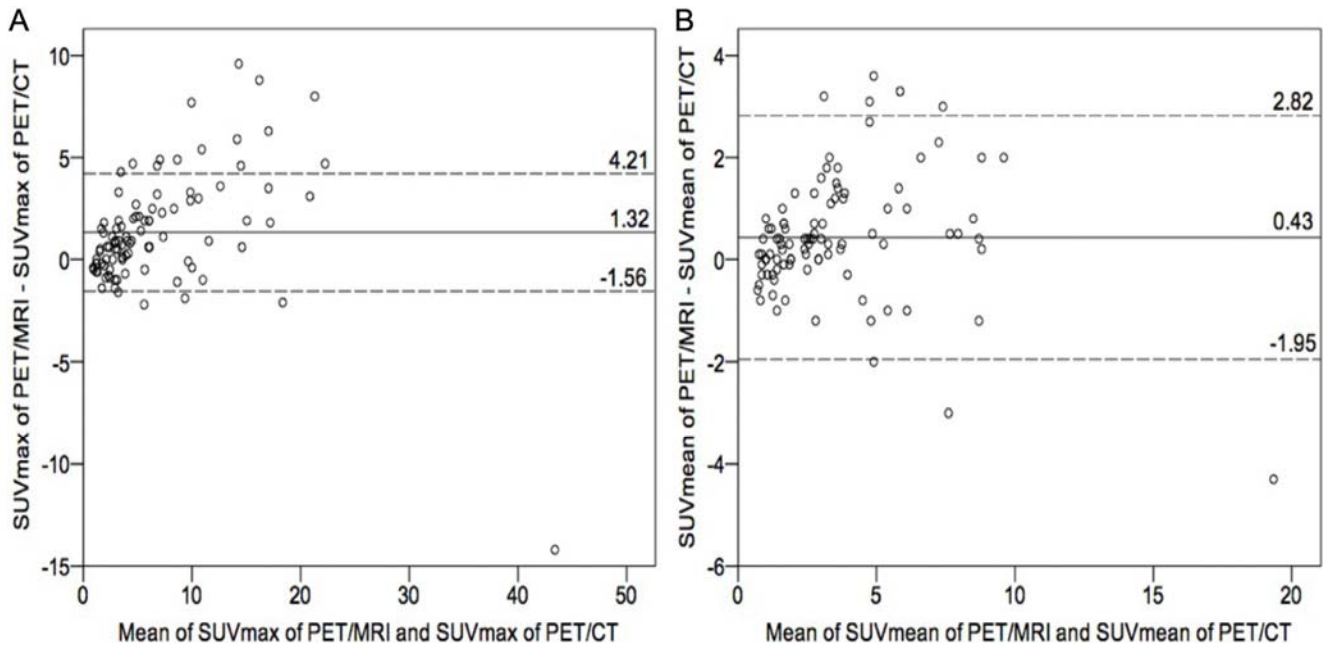


FIGURE 4. Difference between ^{18}F -FDG PET/MRI and ^{18}F -FDG PET/CT regarding SUVmax (A) and SUVmean (B) of 161 corresponding lung lesions illustrated by a Bland-Altman plot. The respective difference between SUV measurements on ^{18}F -FDG PET/MRI and ^{18}F -FDG PET/CT was plotted against their mean. For SUVmax, the mean difference between ^{18}F -FDG PET/MRI and ^{18}F -FDG PET/CT was 1.32; 95 % confidence interval: 4.21 and -1.56 (A). For SUVmean, the mean difference between ^{18}F -FDG PET/MRI and ^{18}F -FDG PET/CT was 0.43; 95 % confidence interval: 2.82 and -1.95 (B).

TABLES

TABLE 1. Tumor entities within the study cohort

Tumor	n
Lung cancer	28
Lymphoma	21
Breast cancer	18
Uterine cancer	12
Ovarian cancer	10
Cancer of unknown primary	8
Malignant melanoma	4
Head and neck cancer	4
Gastrointestinal cancer	3
Malignant mesothelioma	3
Other (< 3 cases / entity)	10

TABLE 2. Categorization of lung lesion dignity on ¹⁸F-FDG PET/CT and ¹⁸F-FDG PET/MRI

Method: total lung lesions detected	Most likely benign	Indeterminate	Suspicious of malignancy
PET/CT: 241	110 (46 %)	31 (13 %)	100 (41 %)
PET/MRI: 161	41 (25 %)	14 (9 %)	106 (66 %)